Theor. Comput. Fluid Dyn.
DOI 10.1007/s00162-011-0233-y

ORIGINAL ARTICLE

Jeroen A. S. Witteveen · Hester Bijl

Transonic velocity fluctuations simulated using extremum diminishing uncertainty quantification based on inverse distance weighting

Received: 15 March 2009 / Accepted: 18 August 2010

Abstract For reliable computational predictions of transonic flows, it is important to resolve the significant effects of physical variations on the shock wave locations. The resulting discontinuities in probability space require extremum diminishing uncertainty quantification to avoid overshoots and undershoots in the response surface approximation. In this paper, the extremum diminishing concept in probability space is extended to infinite parameter domains using inverse distance weighting interpolation of deterministic samples. Based on results for three analytical test functions, the combination of Halton sampling and power parameter limit value $c \to \infty$ is selected. The approach is employed to model spatial-free-stream velocity fluctuations in the highly sensitive transonic AGARD 445.6 wing test case in an up to ten-dimensional probability space. The 0.5% input variations are amplified to a coefficient of variation for the wave drag of $\mathrm{cv_D} = 9.58\%$ in combination with an increase of the mean drag by 1.75% compared to the deterministic value.

Keywords Uncertainty quantification · Inverse distance weighting · Transonic flow · Extremum diminishing

1 Introduction

Physical variability present in practically all engineering problems is in computational fluid dynamics usually not taken into account in a systematic way. These intrinsic variations in, for example, atmospheric conditions and geometrical properties result in varying model parameter values, and initial and boundary conditions. The inherent variability can also be interpreted as uncertainty in terms of a random description in a probabilistic mathematical framework. Physical or aleatoric uncertainty differs in that sense from epistemic uncertainty, caused by modeling unknowns or insufficient input data, which is in general not random in nature.

The effect of physical variations can, nonetheless, be significantly larger than the numerical errors for flow problems which are sensitive to changes in the input data. The aerodynamic drag in the transonic flow regime is, for example, known to be sensitive to small free-stream fluctuations. The resulting variations in the shock wave location lead to an increased variability of local pressures in the shock region. It is, therefore, important to quantify the effect of physical uncertainties in transonic flow problems using robust uncertainty quantification

Communicated by Zang.

The presented work is supported by the NODESIM–CFD project (Non-Deterministic Simulation for CFD based design methodologies); a collaborative project funded by the European Commission, Research Directorate–General in the 6th Framework Programme, under contract AST5–CT–2006–030959.

J. A. S. Witteveen (✉)
Center for Turbulence Research, Stanford University, Building 500, Stanford, CA 94305–3035, USA
E-mail: jasw@stanford.edu

H. Bijl
Faculty of Aerospace Engineering, Delft University of Technology, Kluyverweg 1, 2629 HS Delft, The Netherlands

Published online: 06 July 2011

methods which can deal with discontinuities in a reliable way.

Monte Carlo simulation [10] and Polynomial Chaos methods [1,8,31,32,36] are popular approaches for the detailed and quantitative probabilistic modeling of physical variations by random parameters. The Polynomial Chaos framework has become a well-established spectral method for probability space [9,17,22,24,39]. It has been applied to various problems involving flow [18,20,38] and fluid-structure interaction [33,37]. The mathematical formulation of the Polynomial Chaos problem for output of interest $u(\mathbf{x}, t, \mathbf{a}(\omega))$ is

$$\mathcal{L}(\mathbf{x}, t, \mathbf{a}(\omega); u(\mathbf{x}, t, \mathbf{a}(\omega))) = \mathcal{S}(\mathbf{x}, t, \mathbf{a}(\omega)), \tag{1}$$

with appropriate initial and boundary conditions. Operator $\mathcal{L}$ and source term $\mathcal{S}$ are defined on domain $D{\times}T{\times}A$, where $\mathbf{x} \in D$ and $t \in T$ are the spatial and temporal dimensions with $D \subset \mathbb{R}^d$, $d = \{1, 2, 3\}$, and $T \subset \mathbb{R}^+$. The randomness is introduced in (1) and its initial and boundary conditions by n_a uncorrelated second-order random parameters $\mathbf{a}(\omega) = \{a_1(\omega), \ldots, a_{n_a}(\omega)\} \in A$ with probability density $f_{\mathbf{a}}(\mathbf{a})$ and parameter space $A \subset \mathbb{R}^{n_a}$. The argument ω is a random event with the set of outcomes $\Omega = [0, 1]^{n_a}$ of the probability space $(\Omega, \mathcal{F}, P)$ with $\mathcal{F} \subset 2^{\Omega}$ the σ–algebra of events and P a probability measure. Spatially correlated data is in this framework modeled by random fields, which can be discretized in terms of uncorrelated random parameters using the Karhunen–Loève expansion of the covariance function [15].

Here, we consider nonintrusive uncertainty quantification methods l which construct a weighted approximation $w(\mathbf{x}, t, \mathbf{a})$ of response surface $u(\mathbf{x}, t, \mathbf{a})$ based on n_s deterministic solutions $v_k(\mathbf{x}, t) \equiv u(\mathbf{x}, t, \mathbf{a}_k)$ of (1) for different parameter values $\mathbf{a}_k \equiv \mathbf{a}(\omega_k)$ with $k = 1, \ldots, n_s$. The samples $v_k(\mathbf{x}, t)$ can be obtained by solving the deterministic problem

$$\mathcal{L}(\mathbf{x}, t, \mathbf{a}_k; v_k(\mathbf{x}, t)) = \mathcal{S}(\mathbf{x}, t, \mathbf{a}_k), \tag{2}$$

for $k = 1, \ldots, n_s$, by reusing an existing deterministic flow solver based on standard spatial discretization methods and time marching schemes. A nonintrusive uncertainty quantification method l is then a combination of a sampling method g and an interpolation method h. Sampling method g defines the n_s sampling points $\{\mathbf{a}_k\}_{k=1}^{n_s}$ and it returns the deterministic samples $\mathbf{v}(\mathbf{x}, t) = \{v_1(\mathbf{x}, t), \ldots, v_{n_s}(\mathbf{x}, t)\}$. In nonintrusive Polynomial Chaos methods [11,27], (pseudo-)random sampling and quasi-random sampling techniques are employed such as Latin Hypercube sampling or Hammersley sampling [10]. Sampling in suitable Gauss quadrature points is used in Stochastic Collocation approaches [2,16,21,29]. Interpolation method h results for nonintrusive Polynomial Chaos and Stochastic Collocation in a global polynomial interpolation $w(\mathbf{x}, t, \mathbf{a})$ based on exact Lagrange interpolation through the samples or Least Squares approximation [12]. We are eventually interested in an approximation of the probability distribution and statistical moments $\mu_{\mathrm{u}_i}(\mathbf{x}, t)$ of the output $u(\mathbf{x}, t, \mathbf{a})$, which can be obtained by sorting and weighted integration of $w(\mathbf{x}, t, \mathbf{a})$

$$\mu_{\mathrm{u}_i}(\mathbf{x}, t) \approx \mu_{\mathrm{w}_i}(\mathbf{x}, t) = \int_A w(\mathbf{x}, t, \mathbf{a})^i f_{\mathbf{a}}(\mathbf{a}) \mathrm{d}\mathbf{a}. \tag{3}$$

This information can be used for reducing design safety factors and robust design optimization, in contrast to reliability analysis, in which the probability of failure is of interest [23].

The global polynomial approximation $w(\mathbf{x}, t, \mathbf{a})$ of discontinuous responses in probability space can result in overshoots and undershoots at the discontinuity. Overshoots and undershoots refer here to an interpolation that attains locally alternating higher and lower values than the exact solution due to an oscillatory polynomial fit through the sampling points. These oscillatory predictions can even lead to unphysical realizations. A more robust approximation is pursued by adaptive finite elements discretizations of probability space [7,19,30], which evaluate integral (3) by dividing parameter space A into n_{e} elements A_j

$$\mu_{\mathrm{w}_i}(\mathbf{x}, t) = \sum_{j=1}^{n_{\mathrm{e}}} \int_{A_j} w(\mathbf{x}, t, \mathbf{a})^i f_{\mathbf{a}}(\mathbf{a}) \mathrm{d}\mathbf{a}. \tag{4}$$

Approximation $w(\mathbf{x}, t, \mathbf{a})$ is then a piecewise polynomial function based on local nonintrusive Polynomial Chaos or Stochastic Collocation approaches in usually hypercube elements. In case of higher-order approximations, these finite elements discretizations of probability space still allow local unphysical oscillations. Multielement methods based on a piecewise polynomial approximation of the response in parameter space are also limited to finite parameter domains.

For reliable approximations of discontinuous response surfaces, it is important to define the robustness of uncertainty quantification methods more precisely. This is essential especially for high dimensional probability spaces, for which a response surface approximation can no longer easily be inspected visually. In the field of deterministic finite volume methods there has been much attention for the robust approximation of discontinuities in physical space, which has resulted in the introduction of the extremum diminishing (ED) and local extremum diminishing (LED) concepts [13]. In that context, the ED property ascertains that no unphysical solutions are predicted due to overshoots and undershoots near, for example, shock waves.

The ED concept was recently also extended to probability space as basis for the development of robust uncertainty quantification methods [35]. In probability space, the ED property assures that an uncertainty quantification method does not predict nonzero probabilities for unphysical realization due to overshoots and undershoots in the vicinity of discontinuities. A fourth-order multielement uncertainty quantification method based on Newton–Cotes quadrature points in simplex elements was also proposed which satisfies the requirements of the ED concept in probability space [34,35].

The applicability of this multielement ED uncertainty quantification method is, however, limited to finite parameter domains. Uncertain parameters are often modeled using random parameters with probability distributions on (semi-)infinite parameter ranges. For example, the Gaussian distribution is commonly assumed as a result of the central limit theorem. The Karhunen–Loève expansion for discretizing random fields is also based on Gaussian random parameters. For physically positive parameters often lognormal or Weibull distributions with a semi-infinite parameter domains are used. Although infinite parameter values can be impractical, the truncation of the parameter range at an arbitrary finite value in the multielement ED method introduces a stochastic bias in the simulation results.

In this paper, the extension of the ED concept in probability space to infinite parameter domains is explored in application to velocity fluctuations in transonic flow. An ED uncertainty quantification method for infinite parameter domains is developed based on inverse distance weighing interpolation h of deterministic samples $\mathbf{v}$. Inverse distance weighting (IDW) is an efficient method for multivariate interpolation of scattered data points [28]. It is commonly used for fitting a continuous surface through irregularly spaced data in the generation of contour maps in, for example, geography [3], meteorology [6], and hydrology [4]. Here, inverse distance weighting is employed to construct an interpolation h which is extremum conserving on infinite parameter domains with respect to the samples $\mathbf{v}$. The resulting uncertainty quantification method l is then extremum diminishing with respect to the exact response surface $u(\mathbf{x}, t, \mathbf{a})$. The considered approach can also be used to extend the ED multielement approximation for finite parameter domains to infinite parameter domains by reusing the samples of the multielement formulation.

Extremum diminishing uncertainty quantification for infinite parameter domains is derived in Sect. 2 and the effect of power parameter c in the IDW formulation is analyzed. In Sect. 3.1, the effect of power parameter c is investigated in error convergence studies for three standard test functions based on one random parameter and uniform sampling. The limiting case $c \to \infty$ is applied to the test functions in a two-dimensional probability space in combination with Halton sampling in Sect. 3.2. In Sect. 4, free-stream velocity fluctuations are modeled in the three-dimensional transonic AGARD 445.6 wing problem. First, the effect of a fully correlated inflow velocity on the surface pressure and the wave drag is considered. These results are subsequently compared to cases for velocity fields with strong and weak spatial correlation, which are discretized using an up to ten-dimensional Karhunen–Loève expansion. In Sect. 5, the paper is concluded with a discussion of the main findings.

2 Extremum diminishing uncertainty quantification for infinite parameter domains

In this section, extremum diminishing uncertainty quantification for infinite parameter domains is developed based on inverse distance weighting interpolation. The extremum diminishing concept is defined for probability space in Sect. 2.1. In Sect. 2.2, it is shown that IDW interpolation of samples in probability space satisfies the extremum diminishing property on infinite parameter domains. The effect of the power parameter c is analyzed in Sect. 2.3.

2.1 The extremum diminishing concept in probability space

The extremum diminishing concept has been developed in the context of finite volume methods for a robust approximation of discontinuities in physical space [13]. Here, the extremum diminishing property is defined

for uncertainty quantification methods in probability space with infinite parameter ranges. Consider an uncertainty quantification method l, which results in an approximation $w(\mathbf{x}, t, \mathbf{a})$ of response $u(\mathbf{x}, t, \mathbf{a})$ for an infinite parameter domain $\mathbf{a} \in A$. Let the function $w(\mathbf{x}, t, \mathbf{a})$ be constructed using interpolation h of samples $\mathbf{v}$ generated by sampling method g. In the following, the arguments $\mathbf{x}$ and t are omitted for convenience in the notation. The extremum diminishing property in probability space is then defined as follows.

Definition 1 (*Extremum diminishing*) A set of samples $\mathbf{v}$ is extremum diminishing (ED) with respect to response surface $u(\mathbf{a})$ if

$$\min(\mathbf{v}) \geq \min_A(u(\mathbf{a})) \ \wedge \ \max(\mathbf{v}) \leq \max_A(u(\mathbf{a})). \tag{5}$$

Sampling method g is ED, if the resulting set of samples $\mathbf{v}$ is ED for all $u(\mathbf{a})$. Approximation $w(\mathbf{a})$ of response surface $u(\mathbf{a})$ is ED if

$$\min_A(w(\mathbf{a})) \geq \min_A(u(\mathbf{a})) \ \wedge \ \max_A(w(\mathbf{a})) \leq \max_A(u(\mathbf{a})). \tag{6}$$

Uncertainty quantification method l is ED, if the resulting approximation $w(\mathbf{a})$ is ED for all $u(\mathbf{a})$.

It is shown in [35] that any sampling method g is ED. If interpolation method h is extremum conserving with respect to the samples $\mathbf{v}$, then also uncertainty quantification method l is ED. Extremum conserving is defined in probability space as follows.

Definition 2 (*Extremum conserving*) Interpolation $w(\mathbf{a})$ of samples $\mathbf{v}$ is extremum conserving (EC) if

$$\min_A(w(\mathbf{a})) = \min(\mathbf{v}) \ \wedge \ \max_A(w(\mathbf{a})) = \max(\mathbf{v}). \tag{7}$$

Interpolation method h is EC, if the resulting interpolation $w(\mathbf{a})$ is EC for all $\mathbf{v}$.

2.2 Inverse distance weighting interpolation of deterministic samples

In IDW interpolation [28], the surface $w(\mathbf{a})$ is constructed based on the weighted average of the n_s sampled values $\mathbf{v}$ according to

$$w(\mathbf{a}) = \frac{\sum_{k=1}^{n_s} v_k \phi(r_k)}{\sum_{k=1}^{n_s} \phi(r_k)}, \tag{8}$$

with $r_k = \|\mathbf{a} - \mathbf{a}_k\| \geq 0$ the Euclidean distance between $\mathbf{a}$ and sampling point $\mathbf{a}_k$ in parameter space A. The weighting function ϕ is a function of the inverse of the distance r

$$\phi(r) = r^{-c}, \tag{9}$$

with power parameter $c \geq 0$. In the sampling points $\mathbf{a}_k$, the interpolation surface $w(\mathbf{a})$ is not differentiable for low values of the power parameter $0 \leq c < 1$ and smooth for $c > 1$. In more compact notation (8) can be written as

$$w(\mathbf{a}) = \sum_{k=1}^{n_s} v_k \tilde{\phi}(r_k), \tag{10}$$

in terms of normalized weighting function $\tilde{\phi}(r)$

$$\tilde{\phi}(r_k) = \frac{\phi(r_k)}{\sum_{j=1}^{n_s} \phi(r_j)}. \tag{11}$$

It is derived below that IDW interpolation method h leads to an extremum diminishing uncertainty quantification method l for infinite parameter domains. First, a lemma shows that interpolation method h is an exact interpolant.

Lemma 1 *IDW interpolation method h for samples* $\mathbf{v}$ *is exact in the sense that it satisfies interpolation condition* $w(\mathbf{a}_k) = v_k$ *for* $k = 1, \ldots, n_s$.

Proof Consider the limit of (8) for $\mathbf{a} \to \mathbf{a}_k$

$$w(\mathbf{a}_k) = \lim_{\mathbf{a}\to\mathbf{a}_k} w(\mathbf{a}) = \lim_{\mathbf{a}\to\mathbf{a}_k} \frac{\sum_{j=1}^{n_s} v_j r_j^{-c}}{\sum_{j=1}^{n_s} r_j^{-c}} = \lim_{\mathbf{a}\to\mathbf{a}_k} \frac{v_k r_k^{-c}}{r_k^{-c}} = v_k, \tag{12}$$

for $k = 1, \ldots, n_s$. □

The result of this lemma is used to prove that interpolation method h is EC with respect to the samples $\mathbf{v}$.

Theorem 1 *IDW interpolation method h is EC with respect to the samples* $\mathbf{v}$.

Proof Consider the interpolation function $w(\mathbf{a})$ (10)

$$w(\mathbf{a}) = \sum_{k=1}^{n_s} v_k \tilde{\phi}(r_k),$$

in terms of the normalized weighting function $\tilde{\phi}(r_k)$ (11)

$$\tilde{\phi}(r_k) = \frac{\phi(r_k)}{\sum_{j=1}^{n_s} \phi(r_j)} = \frac{r_k^{-c}}{\sum_{j=1}^{n_s} r_j^{-c}}.$$

For $\tilde{\phi}(r_k)$ holds (i)

$$\sum_{k=1}^{n_s} \tilde{\phi}(r_k) = \sum_{k=1}^{n_s} \left(\frac{r_k^{-c}}{\sum_{j=1}^{n_s} r_j^{-c}} \right) = \frac{\sum_{k=1}^{n_s} r_k^{-c}}{\sum_{j=1}^{n_s} r_j^{-c}} = 1, \tag{13}$$

for all $\mathbf{a} \in A$ and (ii) $0 \le \tilde{\phi}(r_k) \le 1$ for all $\mathbf{a} \in A$, since $r_k \ge 0$ for $k = 1, \ldots, n_s$. Then holds for the minimum of interpolation function $w(\mathbf{a})$ using property (i) and (ii)

$$\min_A (w(\mathbf{a})) = \min_A \left(\sum_{k=1}^{n_s} v_k \tilde{\phi}(r_k) \right) \ge \min_A \left(\min_k (v_k) \sum_{k=1}^{n_s} \tilde{\phi}(r_k) \right) = \min(\mathbf{v}). \tag{14}$$

Using the result of Lemma 1

$$w(\mathbf{a}_k) = v_k$$

for $k = 1, \ldots, n_s$ gives

$$\min_k (w(\mathbf{a}_k)) = \min_k (v_k), \tag{15}$$

and in combination with (14)

$$\min_A (w(\mathbf{a})) = \min(\mathbf{v}). \tag{16}$$

Equivalently for the maximum of $w(\mathbf{a})$ holds

$$\max_A (w(\mathbf{a})) = \max(\mathbf{v}). \tag{17}$$

Since (16) and (17) hold for all $\mathbf{v}$, interpolation method h is EC on infinite parameter domains with respect to the samples $\mathbf{v}$ according to Definition 2. □

The extremum diminishing property of uncertainty quantification method l follows from the next corollary.

Corollary 1 *Uncertainty quantification method l which consists of sampling method g and IDW interpolation method h is ED with respect to response surface* $u(\mathbf{a})$.

Proof Any sampling method g is ED

$$\min(\mathbf{v}) \geq \min_A(u(\mathbf{a})) \ \wedge \ \max(\mathbf{v}) \leq \max_A(u(\mathbf{a})). \tag{18}$$

Theorem 1 then gives

$$\min_A(w(\mathbf{a})) = \min(\mathbf{v}) \geq \min_A(u(\mathbf{a})) \ \wedge \ \max_A(w(\mathbf{a})) = \max(\mathbf{v}) \leq \max_A(u(\mathbf{a})). \tag{19}$$

Since (19) holds for all $u(\mathbf{a})$, uncertainty quantification method l is ED on infinite parameter domains with respect to response $u(\mathbf{a})$ according to Definition 1. □

Theorem 1 also results in an error bound for the error $\varepsilon_\mu = |\mu_\mathrm{w} - \mu_\mathrm{u}|$ in the approximation μ_w of the mean μ_u given by (3) with $i = 1$

$$\mu_\mathrm{w} = \int_A w(\mathbf{a}) f_\mathbf{a}(\mathbf{a}) \mathrm{d}\mathbf{a} = \int_A \frac{\sum_{k=1}^{n_s} v_k r_k^{-c}}{\sum_{k=1}^{n_s} r_k^{-c}} f_\mathbf{a}(\mathbf{a}) \mathrm{d}\mathbf{a}. \tag{20}$$

Corollary 2 *The error $\varepsilon_\mu = |\mu_\mathrm{w} - \mu_\mathrm{u}|$ in the approximation μ_w of the mean μ_u is bounded by $\varepsilon_\mu \leq \max_A(u(\mathbf{a})) - \min_A(u(\mathbf{a}))$.*

Proof For probability density function, $f_\mathbf{a}(\mathbf{a})$ holds $\int_A f_\mathbf{a}(\mathbf{a})\mathrm{d}\mathbf{a} = 1$ and $f_\mathbf{a}(\mathbf{a}) \geq 0$ for all $\mathbf{a} \in A$. The approximation μ_w (20) of the mean is then bounded by

$$\mu_\mathrm{w} = \int_A w(\mathbf{a}) f_\mathbf{a}(\mathbf{a}) \mathrm{d}\mathbf{a} \geq \int_A \min_A(w(\mathbf{a})) f_\mathbf{a}(\mathbf{a}) \mathrm{d}\mathbf{a} = \min_A(w(\mathbf{a})) \geq \min_A(u(\mathbf{a})), \tag{21}$$

where the result of Corollary 1 is used and, equivalently,

$$\mu_\mathrm{w} \leq \max_A(u(\mathbf{a})). \tag{22}$$

Since the exact mean μ_u is also bounded by

$$\mu_\mathrm{u} = \int_A u(\mathbf{a}) f_\mathbf{a}(\mathbf{a}) \mathrm{d}\mathbf{a} \geq \int_A \min_A(u(\mathbf{a})) f_\mathbf{a}(\mathbf{a}) \mathrm{d}\mathbf{a} = \min_A(u(\mathbf{a})), \tag{23}$$

and

$$\mu_\mathrm{u} \leq \max_A(u(\mathbf{a})), \tag{24}$$

the error $\varepsilon_\mu = |\mu_\mathrm{w} - \mu_\mathrm{u}|$ in the approximation μ_w of the mean μ_u is bounded by

$$\varepsilon_\mu \leq \max_A(u(\mathbf{a})) - \min_A(u(\mathbf{a})). \tag{25}$$

□

The error in the mean approximation μ_w is, therefore, bounded by the difference between the minimum and maximum of the exact response surface $u(\mathbf{a})$. If the exact response $u(\mathbf{a})$ is a constant function, then the approximation $w(\mathbf{a})$ is exact with $\varepsilon_\mu = 0$.

2.3 Analysis of power parameter c

Power parameter c can be used to influence the accuracy of the interpolation function $w(\mathbf{a})$ and the resulting approximation of the statistical moments (3). Below, the two limiting cases $c = 0$ and $c \to \infty$ are considered. For $c = 0$ holds

$$w(\mathbf{a})|_{c=0} = \left. \frac{\sum_{k=1}^{n_s} v_k r_k^{-c}}{\sum_{k=1}^{n_s} r_k^{-c}} \right|_{c=0} = \frac{1}{n_s} \sum_{k=1}^{n_s} v_k, \tag{26}$$

which is equal to the arithmetic mean of the samples $\mathbf{v}$ independent of $\mathbf{a}$. The mean μ_{w} is then equal to the mean of the samples $\mu_{\mathbf{v}}$ and the standard deviation σ_{w} is by definition equal to zero. A better approximation is given by the limit $c \to \infty$

$$\lim_{c\to\infty} w(\mathbf{a}) = \lim_{c\to\infty} \left(\frac{\sum_{k=1}^{n_s} v_k r_k^{-c}}{\sum_{k=1}^{n_s} r_k^{-c}} \right) = v_j, \tag{27}$$

with j for which holds

$$r_j(\mathbf{a}) = \min_k (r_k(\mathbf{a})). \tag{28}$$

The interpolation value $w(\mathbf{a})$ in a point $\mathbf{a}$ in parameter space A is then equal to the sampled value v_j in the nearest sampling point $\mathbf{a}_j$. The limit case for $c \to \infty$, therefore, corresponds to nearest neighbor interpolation. This results for moment approximation (3) in

$$\mu_{\mathrm{w}_i} = \int_A w(\mathbf{a})^i f_{\mathbf{a}}(\mathbf{a}) \mathrm{d}\mathbf{a} = \sum_{j=1}^{n_s} \int_{A_j} v_j^i f_{\mathbf{a}}(\mathbf{a}) \mathrm{d}\mathbf{a} = \sum_{j=1}^{n_s} v_j^i \int_{A_j} f_{\mathbf{a}}(\mathbf{a}) \mathrm{d}\mathbf{a}, \tag{29}$$

with subdomains $A_j \subset A$ for which holds with $\hat{\mathbf{a}}_j \in A_j$

$$r_j(\hat{\mathbf{a}}_j) = \min_k (r_k(\hat{\mathbf{a}}_j)), \tag{30}$$

for $j = 1, \ldots, n_s$. The moment approximation for the limit case $c \to \infty$ (29) is comparable to the evaluation of the moment relation by multielement methods (4). For $c \to \infty$, the integral over parameter space A is divided into a summation of integrals over n_s polyhedral subdomains A_j defined by (30). The boundary of these subdomains A_j is known as a Voronoi polygon and the resulting discretization of probability space is called a Voronoi diagram [26]. The value of the response surface approximation is constant in each element and equal to the sampled value v_j for sample $\mathbf{a}_j$ in element A_j for $j = 1, \ldots, n_s$.

3 Results for analytical test functions

Extremum diminishing uncertainty quantification for infinite parameter domains is first studied in application to three standard analytical test functions. In Sect. 3.1, an appropriate value of power parameter c is selected based on results for one random parameter and uniform sampling. This parameter value is used in Sect. 3.2 in approximations of the two-dimensional versions of the test functions in combination with Halton sampling.

3.1 Effect of power parameter c

The effect of power parameter c on the approximation accuracy is studied for the step function, arctangent function, and Gaussian function. The step function is used to illustrate the robust approximation of discontinuous responses. The arctangent function is considered as an example of a smooth and monotone function. The approximation of a response surface with a local extremum is studied for the Gaussian function. The randomness is given by $n_a = 1$ random parameter $a_1(\omega)$ with a standard Gaussian distribution with mean $\mu_a = 0$ and standard deviation $\sigma_a = 1$. The sampling g is performed uniform in $\omega \in [0, 1]$. Results for power parameter values $c \in [0, 20]$ and $c \to \infty$ are shown.

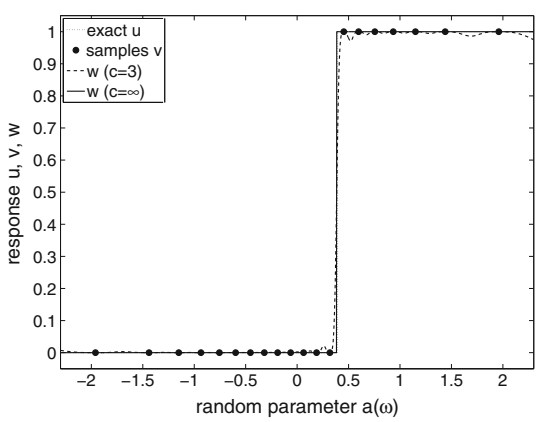

(a) Response surface $u(a_1)$

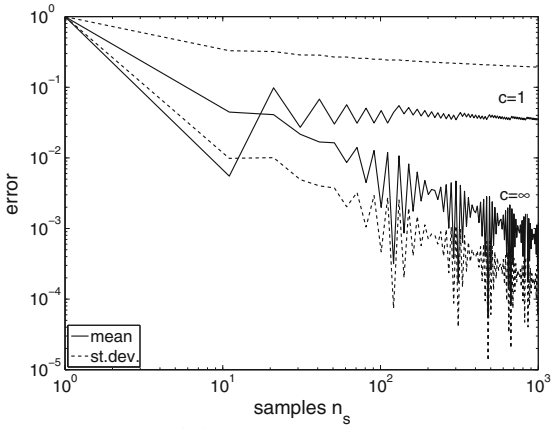

(b) Error convergence

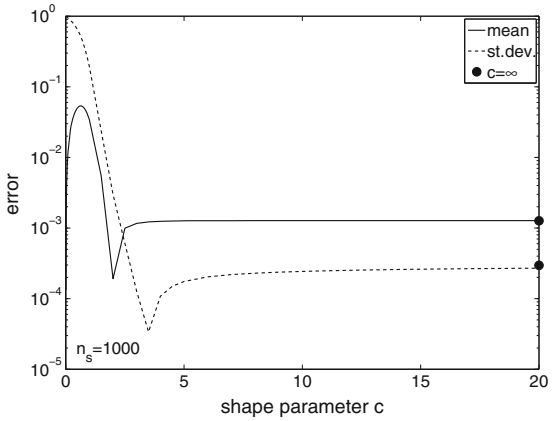

(c) Effect of c

Fig. 1 Approximation of the step function with random parameter $a_1(\omega)$

3.1.1 Step function

A step function with an arbitrary location and orientation of the discontinuity is given by the following Heaviside function

$$u(\mathbf{a}) = H(\mathbf{a} \cdot \bar{\mathbf{a}} - \bar{a}_1^2), \tag{31}$$

with $\bar{\mathbf{a}} = \{\bar{a}_1, \ldots, \bar{a}_{n_a}\}$ a vector of n_a arbitrary numbers in the domain $\bar{a}_i \in [-\frac{1}{2}, \frac{1}{2}]$ for $i = 1, \ldots, n_a$. The function is here introduced in a multidimensional formulation, since it is also used as a two-dimensional test problem in the next section. The approximations of the step function for power parameter values $c = 3$ and $c \to \infty$ based on $n_s = 20$ samples are shown in Fig. 1a. Both approximations show an extremum conserving interpolation of the samples. The error in the piecewise constant approximation for $c \to \infty$ is only a result of the error in the predicted discontinuity location. The interpolation for $c = 3$ exhibits minor extremum conserving oscillations near the discontinuity and in the tails of the distribution.

The error convergence of the mean μ_w and standard deviation σ_w as function of the number of samples n_s is given in Fig. 1b for $c = 1$ and $c = \infty$. The error ε_μ in the approximation of the mean μ_u is here defined as

$$\varepsilon_\mu = \frac{|\mu_\mathrm{w} - \mu_\mathrm{u}|}{|\mu_\mathrm{u}|}, \tag{32}$$

with μ_w the mean that follows from the response surface approximation $w(\mathbf{a})$. The order $\mathcal{O}_\mu$ of the error convergence of ε_μ is then given by the slope of the least-squares interpolation $\tilde{\varepsilon}_\mu(n_s)$ of the error ε_μ as function of the number of samples n_s in the asymptotic region of the logarithmic plot of Fig. 1b

$$\mathcal{O}_\mu = -\frac{\log\left(\frac{\tilde{\varepsilon}_\mu(n_{s_1})}{\tilde{\varepsilon}_\mu(n_{s_2})}\right)}{\log\left(\frac{n_{s_1}}{n_{s_2}}\right)}, \tag{33}$$

with n_{s_1} and n_{s_2} two different sample sizes in the asymptotic range. Equivalent relations are used for the error ε_σ in the standard deviation σ and its order of convergence $\mathcal{O}_\sigma$. The average first order convergence for $c \to \infty$ exhibits an oscillatory behavior due to the approximation of the discontinuity location. The error for $c = 1$ shows a smoother convergence at a significantly slower convergence rate.

The effect of the power parameter is further illustrated in Fig. 1c for $c \in [0, 20]$ and $c \to \infty$ with $n_s = 1{,}000$. For $c = 0$, the error in the standard deviation has a maximum, since the standard deviation is by definition $\sigma_\mathrm{w} = 0$ for $c = 0$ according to (26). For that limit value of the power parameter, the mean μ_w is also equal to the mean of the samples $\mu_\mathbf{v}$. For $c \to \infty$ the error in both the mean ε_μ and standard deviation ε_σ is lower and nearly independent of c. The local minima for the errors in the mean and standard deviation at $c = 2$ and $c = 3.5$, respectively, are related to the oscillatory convergence behavior.

3.1.2 Arctangent function

The arctangent function with n_a arbitrary numbers $\bar{\mathbf{a}}$ is given for $0 \leq u(\mathbf{a}) \leq 1$ by

$$u(\mathbf{a}) = \frac{1}{\pi}\arctan(\mathbf{a}\cdot\bar{\mathbf{a}} - \bar{a}_1^2) + \frac{1}{2}. \tag{34}$$

The approximation of the arctangent function in Fig. 2a gives a staircase behavior for $c \to \infty$ and a smoother interpolation for $c = 3$. For the continuous arctangent function, the error convergence in Fig. 2b is also smooth with again a first order convergence for $c \to \infty$ and a significantly slower convergence rate for $c = 1$. The error decreases in general with increasing power parameter value c in Fig. 2c with a minimum for $c \to \infty$.

3.1.3 Gaussian function

A Gaussian test function with an arbitrary location of the maximum is given by

$$u(\mathbf{a}) = \prod_{i=1}^{n_a} \frac{1}{\sigma\sqrt{2\pi}} \exp\left(\frac{-(a_i - \bar{a}_i)^2}{2\sigma^2}\right), \tag{35}$$

with $\sigma = 1$. The results in Fig. 3 show that shape parameter value $c \to \infty$ results also for the Gaussian function with a local extremum in the minimum error, a staircase approximation of the response, and first order error convergence.

In conclusion, the results for the test functions indicate that power parameter value $c \to \infty$ results in general in the most accurate approximation of the mean and standard deviation. Even for this, optimal power parameter value the error convergence is limited to first order accuracy. This suggests that the extremum diminishing robustness criterion can for infinite parameter domains compromise the efficiency of uncertainty quantification.

3.2 Two-dimensional response surface approximation for $c \to \infty$

Uniform sampling method g employed in the previous section for one random parameter $a_1(\omega)$ results in an exponentially fast increase of the sample size as function of the number of random parameters. More efficient sampling techniques in multiple dimensions are, for example, Monte Carlo sampling, Latin Hypercube sampling, or Halton sampling. It has been verified that these sampling approaches g do not result in significant differences in accuracy of uncertainty quantification method l. Halton sampling is selected in the following, since it is a hierarchical sampling strategy with a good spread of the samples. It is applied to the three test problems with two random input parameters $a_1(\omega)$ and $a_2(\omega)$ in combination with power parameter value $c \to \infty$. Higher dimensional probability spaces are considered in the transonic wing test problem.

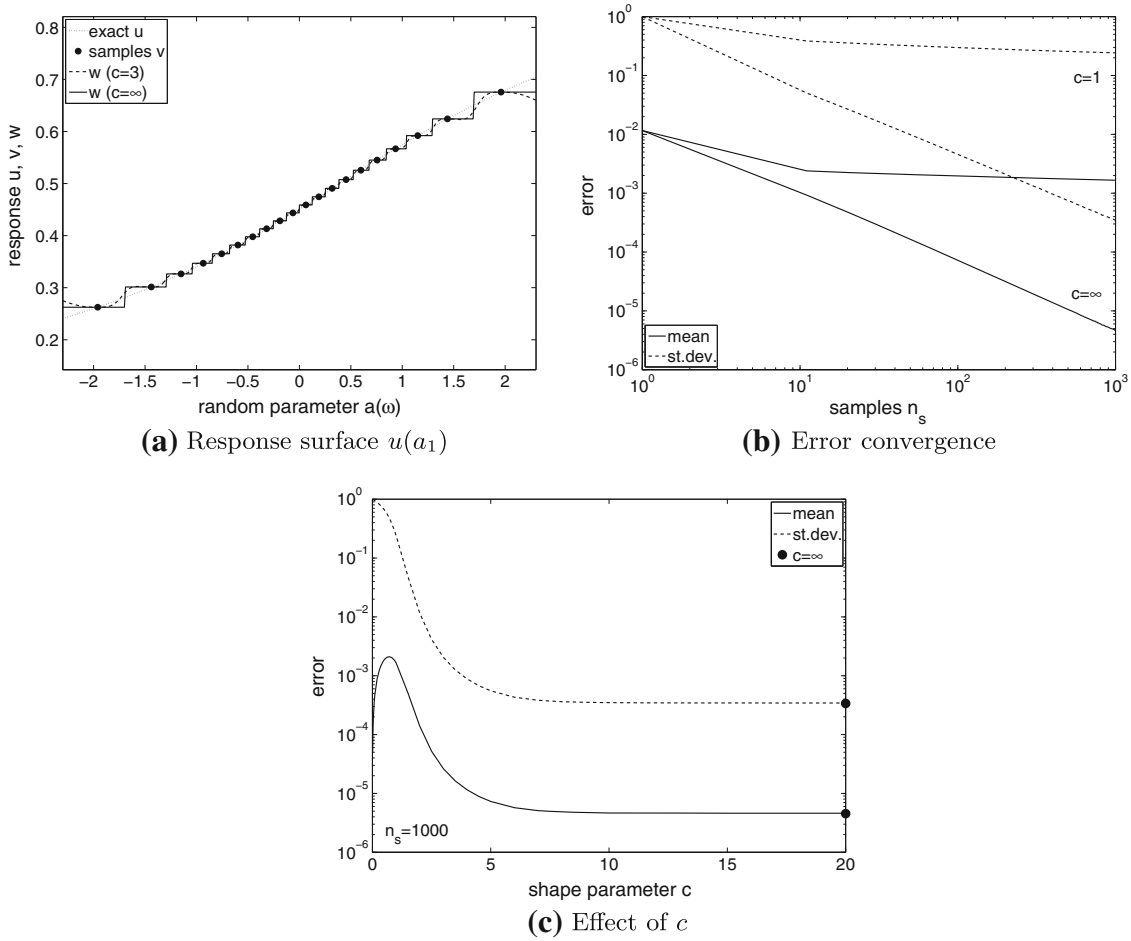

(a) Response surface $u(a_1)$

(b) Error convergence

(c) Effect of c

Fig. 2 Approximation of the arctangent function with random parameter $a_1(\omega)$

3.2.1 Step function

The two-dimensional step function given by (31) with $n_a = 2$ is shown in Fig. 4a. The approximation $w(\mathbf{a})$ based on the extremum conserving interpolation of $n_s = 100$ Halton samples can be found in Fig. 4b. The interpolation predicts a true discontinuity without overshoots and undershoots. The error in the approximation is only caused by the unknown discontinuity location in between the samples. This results again in an irregular convergence behavior shown in Fig. 4c.

3.2.2 Arctangent function

The approximation of the arctangent function in two dimensions is shown in Fig. 5. The multielement Vonoroi diagram character of the piecewise constant interpolation for $c \to \infty$ can clearly by recognized, where each of the polygonal elements contains one of the Halton samples. The error convergence is less smooth than for the one-dimensional problem due to the less regular Halton sampling sequence.

3.2.3 Gaussian function

Figure 6 shows the approximation of the Gaussian response surface in two dimensions. The error convergence with increasing number of samples n_s approaches first order accuracy.

In summary, the two-dimensional results show that also for multiple random parameters the extremum diminishing concept in combination with Halton sampling leads to a robust approximation of discontinuities.

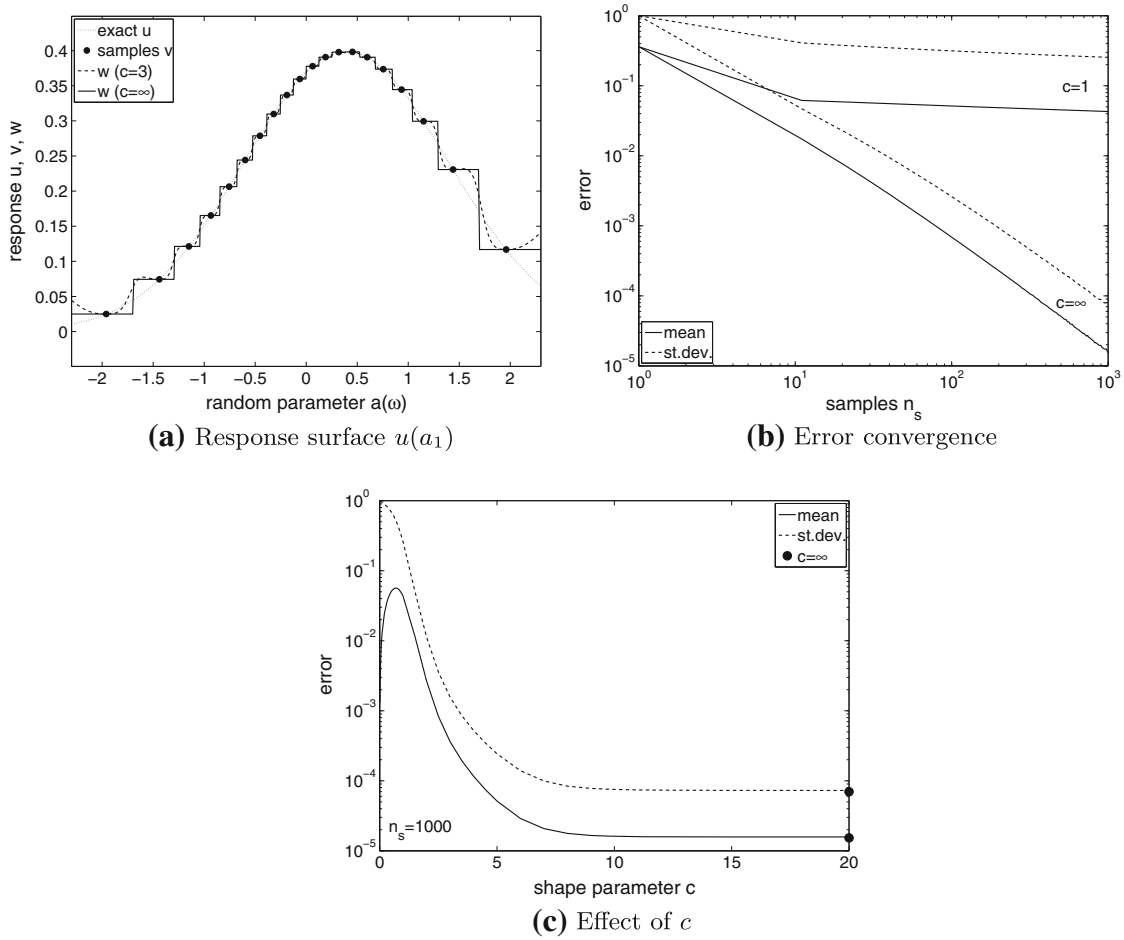

(a) Response surface $u(a_1)$

(b) Error convergence

(c) Effect of c

Fig. 3 Approximation of the Gaussian function with random parameter $a_1(\omega)$

The accuracy is, however, also for smooth response surfaces on infinite parameter domains limited to first order convergence.

4 Effect of transonic velocity fluctuations

Extremum diminishing uncertainty quantification is employed below to study the effect of free-stream velocity variations on the wave drag of the transonic AGARD 445.6 wing. This standard test case for three-dimensional transonic flow is described in Sect. 4.1. A spatially fully correlated velocity field is assumed in Sect. 4.2. In Sects. 4.3 and 4.4, spanwise velocity fluctuations with strong and weak spatial correlation are considered. The AGARD 445.6 wing test case is chosen to study the ED uncertainty quantification method in a challenging CFD problem with highly sensitive transonic flow and shock discontinuities. The problem contains the typical features of computationally intensive deterministic samples and potentially the effects of numerical noise. The application should not primarily be considered as an uncertainty quantification validation.

4.1 Transonic AGARD 445.6 wing

The AGARD 445.6 wind tunnel experiment is defined by a wing with a NACA 65A004 symmetric airfoil, taper ratio of 0.66, 45° quarter-chord sweep angle, and a 2.5-foot semi-span under zero angle of attack [40]. The free-stream conditions for density and pressure are $\rho_\infty = 0.099468\,\text{kg/m}^3$ and $p_\infty = 7704.05\,\text{Pa}$, respectively. The mean free-stream velocity $\mu_{U_\infty} = 312.83\,\text{m/s}$ used here corresponds to a Mach number of $M_\infty = 0.95$. Previous numerical simulations of the AGARD 445.6 wing can be found in [14,41].

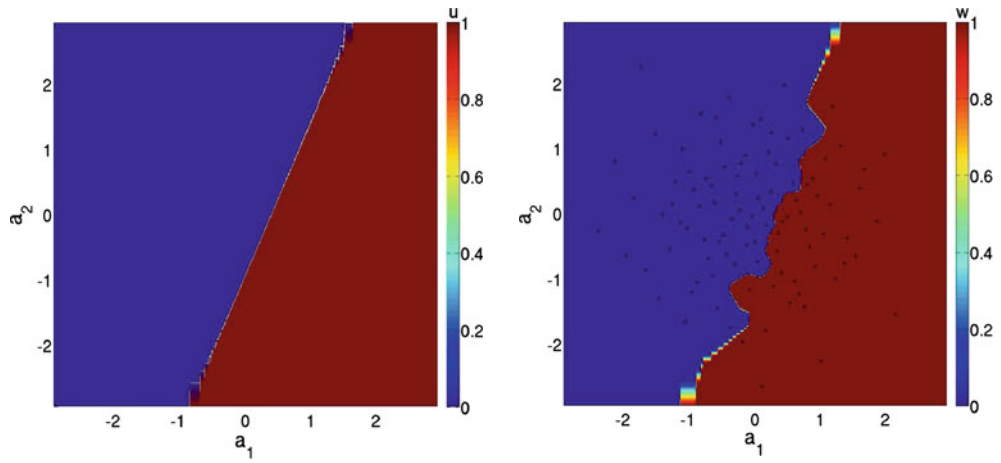

(a) Exact response $u(\mathbf{a})$ **(b)** Approximation $w(\mathbf{a})$

(c) Error convergence

Fig. 4 Approximation of the step function with two random parameters $a_1(\omega)$ and $a_2(\omega)$

The wave drag and the pressure distribution on the wing surface are resolved to give a practical illustration of the robustness of an extremum diminishing approximation of a transonic shock wave sensitive to free-stream variations. The Euler equations for inviscid flow [5] are used to determine the trends in wave drag as a significant contribution to the total drag in the transonic regime. The governing equations are discretized using a second-order Roe upwind finite volume scheme on an unstructured hexahedral mesh in a $60 \times 15 \times 30$ m external flow domain. Based on a grid convergence study for the mean velocity μ_{U_∞}, a mesh with $3.8 \cdot 10^5$ volumes is selected to perform the uncertainty quantification study. The surface mesh is shown in Fig. 7a. The residual is reduced by five orders of magnitude with respect to that of the initial uniform flow solution in typically $2 \cdot 10^3$ iterations. The residual is here defined as the L_2 norm of the residual of the governing system of equations per cell. Smaller cells are given a relatively large contribution to the residual by dividing the cell residuals by the cell volume.

The deterministic solution for the mean free-stream velocity μ_{U_∞} is given in Fig. 7b in terms of the pressure distribution over the wing surface. A strong shock wave downstream of a low pressure supersonic region can be identified close to the trailing edge at the root of the wing. A secondary, weaker shock wave is present near the leading edge in the tip region. A robust uncertainty quantification approach is, therefore, required to resolve the discontinuities in probability space caused by the shock waves in a reliable way. The deterministic computation predicts for zero angle of attack a wave drag of $D = 0.8527$ Newton (N), which corresponds to a wave drag coefficient of $C_\mathrm{D} = 0.4961 \cdot 10^{-3}$ defined as

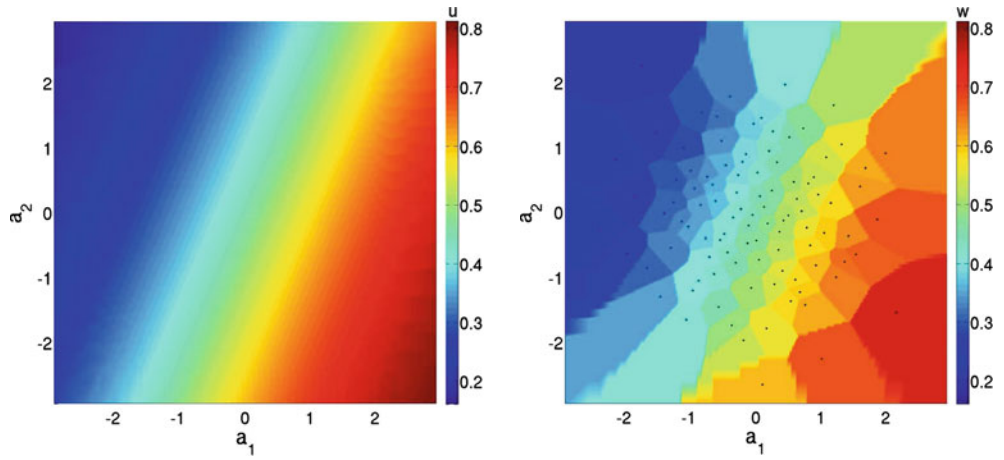

(a) Exact response $u(\mathbf{a})$ **(b)** Approximation $w(\mathbf{a})$

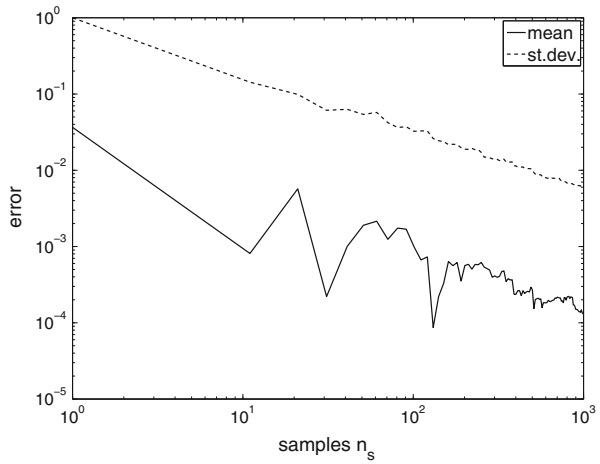

(c) Error convergence

Fig. 5 Approximation of the arctangent function with two random parameters $a_1(\omega)$ and $a_2(\omega)$

$$C_{\mathrm{D}} = \frac{D}{\frac{1}{2}\rho_\infty U_\infty^2 S}, \tag{36}$$

with wing area $S = 0.3531\ \mathrm{m}^2$ and free-stream velocity U_∞ equal to its mean value μ_{U_∞}.

The simulations are performed using the commercial CFD code *Hexstream* of *Numeca Int.* based on an unstructured fully hexahedral finite volume discretization. The upwind scheme is used to minimize the contribution of fictitious numerical drag due to numerical damping. External boundary conditions are imposed on the far field boundaries and the symmetry plane is set to mirror boundary conditions. In spite of the upwind scheme and a proper treatment of the boundary conditions, the effect of fictitious drag cannot entirely be eliminated. However, it has been verified that the numerical drag is small compared to the predicted wave drag through a mesh convergence study.

4.2 Fully correlated velocity field

A simplified model for atmospheric velocity fluctuations is to treat the free-stream velocity $U_\infty(\omega)$ in the inflow boundary conditions as a random parameter with full spatial correlation. The velocity is assumed to have a Gaussian distribution with coefficient of variation $\mathrm{cv}_{\mathrm{U}_\infty} = 0.5\%$, since the Karhunen–Loève expansion used in the next sections is also based on normal random parameters. The coefficient of variation $\mathrm{cv}_{\mathrm{U}_\infty}$ is here defined as the ratio of the standard deviation $\sigma_{\mathrm{U}_\infty}$ and the mean μ_{U_∞} of the free-stream velocity

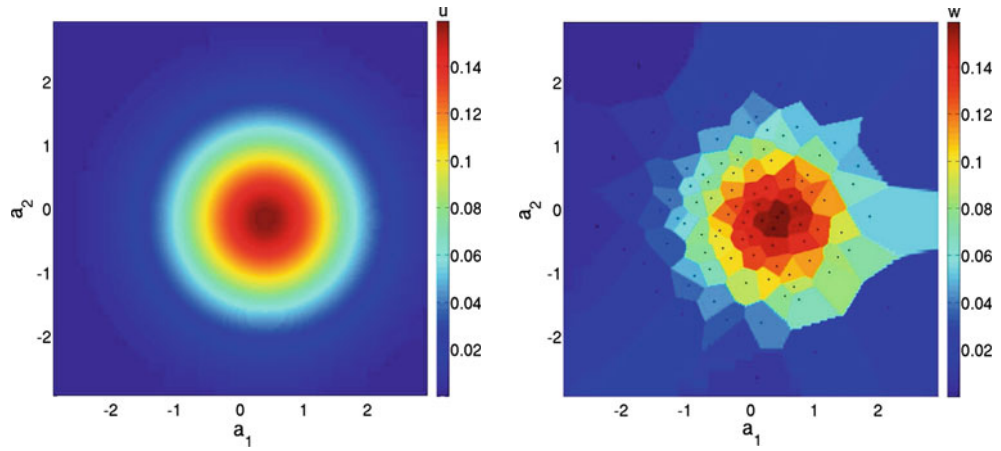

(a) Exact response $u(\mathbf{a})$ **(b)** Approximation $w(\mathbf{a})$

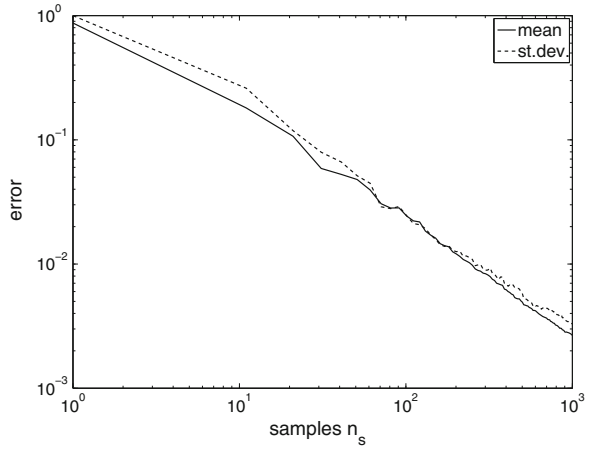

(c) Error convergence

Fig. 6 Approximation of the Gaussian function with two random parameters $a_1(\omega)$ and $a_2(\omega)$

$$\mathrm{cv}_{\mathrm{U}_\infty} = \frac{\sigma_{\mathrm{U}_\infty}}{\mu_{\mathrm{U}_\infty}}, \tag{37}$$

with $\mu_{U_\infty} = 312.83$ m/s. Due to the low input variation, all samples used below fall within an interval around the deterministic value $U_\infty \in [309, 316]$ in the transonic regime. It is nonetheless important to model the tails of the distribution, since truncating them arbitrarily would result in a bias error in the stochastic results.

The effect of random free-stream velocity $U_\infty(\omega)$ is resolved using up to $n_s = 50$ Halton samples and interpolation with shape parameter value $c \to \infty$. Results for the mean and standard deviation of the surface pressure field are given in Fig. 8a, b. The effect of the velocity variation is concentrated in the shock region with lower gradients in the mean pressure field than in the deterministic case and an increased variability of local pressures. This results in a maximum coefficient of variation in the surface pressure of $\mathrm{cv}_\mathrm{p} = 4.46\%$, which is defined as

$$\mathrm{cv}_\mathrm{p} = \max_{\mathbf{x}\in X} \frac{\sigma_\mathrm{p}(\mathbf{x})}{\mu_\mathrm{p}(\mathbf{x})}, \tag{38}$$

with $\mathbf{x} \in X$ a spatial parameterization of the wing surface. This corresponds to an amplification of the input coefficient of variation by a factor 8.92. The amplification is caused by the effect that small variations in shock wave location caused by the random free-stream velocity lead locally to large jumps in surface pressure.

Downstream of both shock waves the standard deviation attains also a secondary local maximum. As a result of the extremum diminishing property, this phenomenon cannot be an artificial effect caused by overshoots

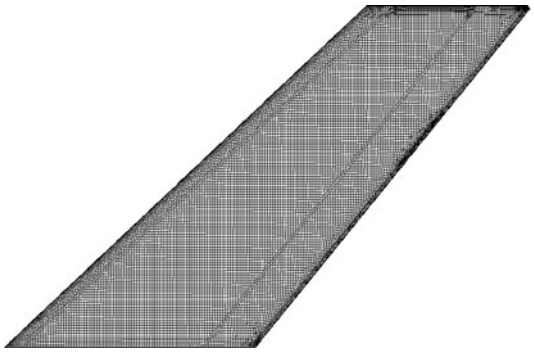

(a) Surface mesh

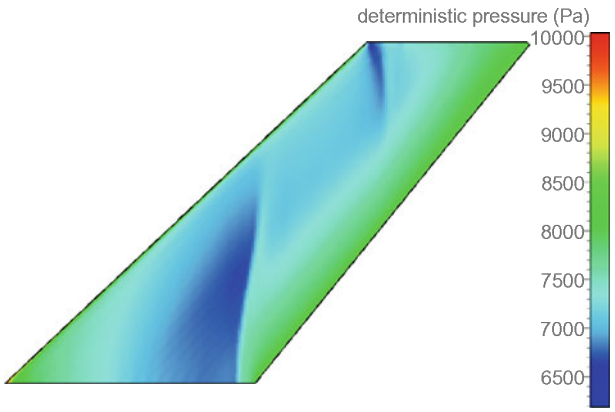

(b) Pressure distribution

Fig. 7 Deterministic AGARD 445.6 wing

Table 1 Wave drag of the AGARD 445.6 wing for $n_s = 50$ and $n_{\mathrm{KL}} = 5$

Velocity	Mean μ_{D}	Standard deviation σ_{D}	Variation cv_{D}
Deterministic	0.8527N	–	–
Full correlation	0.8676N	0.08315N	9.58%
Strong correlation	0.8631N	0.07538N	8.73%
Weak correlation	0.8555N	0.05008N	5.85%

and undershoots in the uncertainty quantification interpolation near the shock wave. It is actually associated with the Zierep post-shock expansion commonly predicted by Euler solvers [25].

The variability in the local pressure field also affects the wave drag of the wing. The resulting mean drag of $\mu_{\mathrm{D}} = 0.8676\mathrm{N}$ is 1.75% higher than the deterministic value, see Table 1. The standard deviation of $\sigma_{\mathrm{D}} = 0.08315\mathrm{N}$ results in a coefficient of variation of $\mathrm{cv}_{\mathrm{D}} = \sigma_{\mathrm{D}}/\mu_{\mathrm{D}} = 9.58\%$. The amplification of input variability by a factor 19.2 illustrates that it is of practical importance to develop robust uncertainty quantification to be able to resolve the effect of randomness in highly sensitive problems with transonic shock waves reliably.

The convergence of the mean and standard deviation with increasing number of samples n_s is shown in Fig. 9a, b. A staircase behavior can be recognized in the convergence of both the mean and standard deviation. This indicates that the approximation of the mean and standard deviation changes more by adding certain samples compared to the other samples. By inspection it follows that a sample has the most effect on the moment approximations, if it corresponds to a velocity realization that is lower or higher than all previously sampled free-stream velocities. This can be understood from the observation that the deterministic solution for the lowest and highest sampled velocity are used in both the interpolation and the extrapolation of the one-dimensional response surface to the tails of the distribution. The other samples are only used in interpolating

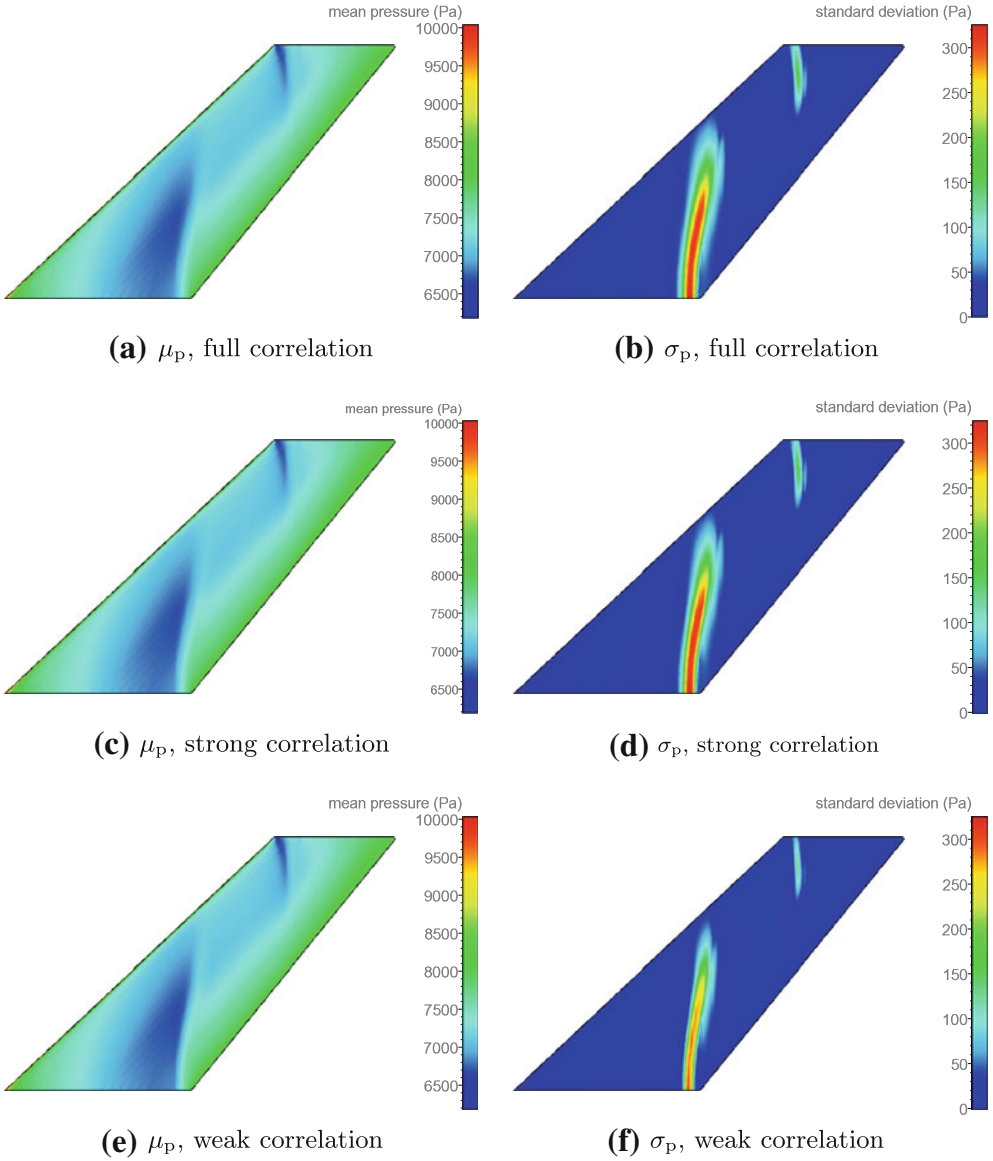

Fig. 8 Mean μ_p and standard deviation σ_p of the surface pressure distribution in Pascal (Pa) with $n_s = 50$ and $n_{KL} = 5$ for the AGARD 445.6 wing subject free-stream velocity fluctuations with: (**a**, **b**) full, (**c**, **d**) strong, and (**e**, **f**) weak spatial correlation

the response surface in between the samples. One might, therefore, consider other sampling strategies, which sample more in the tails of the probability distribution, to increase the number of samples near the extremes of the velocity distribution. This can increase the convergence of the method.

4.3 Strong spatial correlation

For a more realistic modeling of atmospheric velocity fluctuations, its spatial correlation structure should be taken into account. Here, it is assumed that the spatial correlation of the Gaussian random field is given by the commonly used exponential covariance function

$$C(x_1, x_2) = \mathrm{e}^{-\frac{|x_1 - x_2|}{L_c}}, \tag{39}$$

with L_c the correlation length. Correlated random fields are often discretized by a set of uncorrelated random parameters using a Karhunen–Loève (KL) expansion [15]. This is a mean error minimizing expansion of the

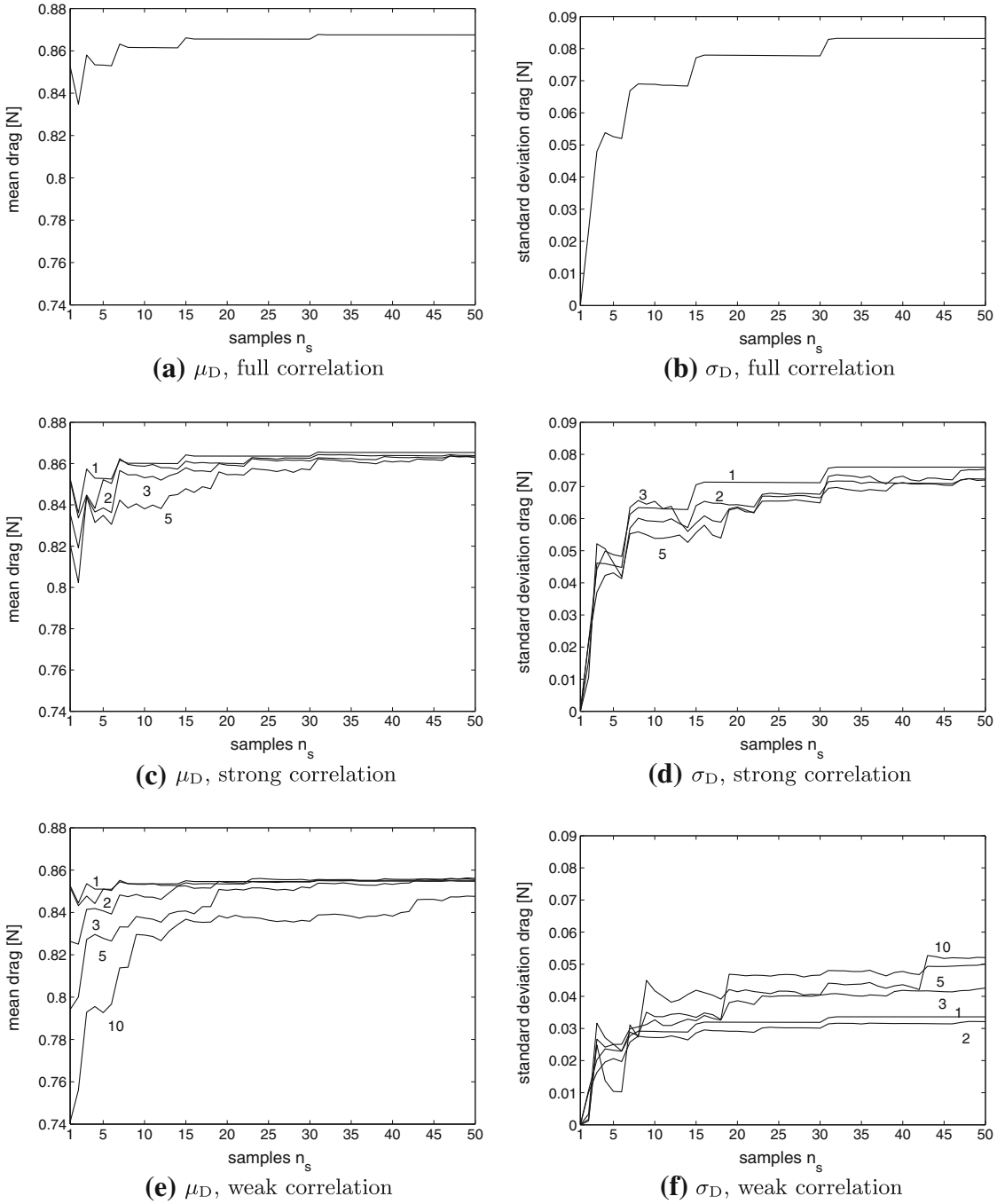

(a) μ_{D}, full correlation **(b)** σ_{D}, full correlation

(c) μ_{D}, strong correlation **(d)** σ_{D}, strong correlation

(e) μ_{D}, weak correlation **(f)** σ_{D}, weak correlation

Fig. 9 Convergence of the mean μ_{D} and standard deviation σ_{D} of the drag in Newton (N) as function of the number of samples n_s for the AGARD 445.6 wing subject to free-stream velocity fluctuations modeled with varying number of Karhunen–Loève expansion terms $n_{\mathrm{KL}} = \{1, 2, 3, 5, 10\}$

covariance function in terms of its eigenfunctions. For the exponential covariance function, the KL expansion on spatial domain $x \in [-b, b]$ is given analytically by [8]

$$w(x, \omega) = \sum_{n=0}^{\infty} \sqrt{\lambda_n} a_n(\omega) f_n(x), \tag{40}$$

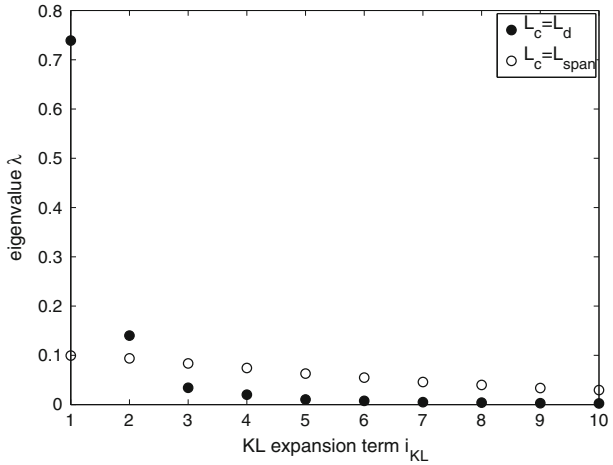

Fig. 10 Karhunen–Loève eigenvalues for a long and short correlation length, L_d and L_span, respectively

with standard Gaussian random parameters $a_n(\omega)$ and eigenvalues

$$\lambda_n = \frac{2d}{\omega_n^2 + d^2}, \qquad \lambda_n^* = \frac{2d}{\omega_n^{*2} + d^2}, \tag{41}$$

with $d = 1/L_\mathrm{c}$, where λ_n and λ_n^* hold for even n and odd n, respectively, and corresponding eigenfunctions

$$f_n(x) = \frac{\cos(\omega_n x)}{\sqrt{b + (1/2\omega_n)\sin(2\omega_n b)}}, \qquad f_n^*(x) = \frac{\sin(\omega_n^* x)}{\sqrt{b - (1/2\omega_n^*)\sin(2\omega_n^* b)}}. \tag{42}$$

The values of ω_n and ω_n^* can be found by solving the transcendental equations

$$d - \omega\tan(\omega b) = 0, \qquad \omega^* + d\tan(\omega^* b) = 0. \tag{43}$$

Here, the spatial variations in the spanwise direction are modeled, since they are expected to have the largest effect. In the vertical direction, the velocity boundary condition is assumed to be fully correlated. In order to avoid boundary effects, the KL expansion is constructed on the domain $x \in [-L_\mathrm{d}, L_\mathrm{d}]$, with the root of the wing in the origin and L_d the width of the computational flow domain. First, a strongly correlated velocity field is considered with correlation length $L_\mathrm{c} = L_\mathrm{d} = 15$ m.

In numerical applications, the KL expansion (40) needs to be truncated at a finite number of terms n_KL. The truncation then determines the number $n_a = n_\mathrm{KL}$ of uncorrelated random parameters $a_n(\omega)$ in the discretization and, consequently, the dimensionality of the probability space. In Fig. 10, the first 10 eigenvalues are shown for the strong correlation case $L_\mathrm{c} = L_\mathrm{d}$ in comparison to those for weak correlation discussed in the next section. Since for $L_\mathrm{c} = L_\mathrm{d}$ the eigenvalues decay rapidly for increasing n_KL, a discretization with up to $n_\mathrm{KL} = 5$ KL-expansion terms is used.

The resulting mean and standard deviation fields of the surface pressure are given in Fig. 8c, d for $n_s = 50$ samples and $n_\mathrm{KL} = 5$. The results for the strongly correlated case correspond with a maximum coefficient of variation of $\mathrm{cv_p} = 4.47\%$ closely to the fully correlated case. This illustrates that the effect of the randomness is also robustly resolved in the five-dimensional probability space originating from the KL expansion.

The mean and standard deviation of the drag are shown in Fig. 9c, d for $n_\mathrm{KL} = \{1, 2, 3, 5\}$. The mean drag converges for $n_s = 50$ samples and $n_\mathrm{KL} = 5$ to a value of $\mu_\mathrm{D} = 0.8631$N, which is in between the deterministic drag and the fully correlated prediction. From the comparison with the discretizations with $n_\mathrm{KL} = \{1, 2, 3\}$ it can be concluded that the initial error and the number of samples that is required to reach convergence increases with increasing dimensionality of the probability space. The standard deviation of $\sigma_\mathrm{D} = 0.07538$N is 9.35% lower than for the fully correlated case.

4.4 Weak spatial correlation

It is unlikely that the relevant atmospheric velocity fluctuations are correlated with the user defined dimensions of the external flow domain. More interesting is the effect of velocity variations which are correlated with a characteristic length of the wing. A significantly lower correlation length corresponding to the semi-span of the wing $L_c = L_{span} = 0.762$m is, therefore, used in this section. Due to the weaker correlation, the eigenvalues (41) in the KL expansion decrease significantly slower than for the $L_c = L_d$ case as shown in Fig. 10. This well-known decreasing efficiency of the KL expansion with decreasing correlation length leads to an increasing number of required expansion terms and, consequently, higher dimensional probability spaces.

For comparison with the previous results, $n_{KL} = 5$ expansion terms are taken into account in the approximation of the mean and standard deviation of the surface pressure field in Fig. 8e, f. Although the results show a comparable qualitative pattern, the predicted maximum coefficient of variation of $cv_p = 4.31\%$ is significantly lower than in the previous cases. This effect is caused by the underestimation of the input variability by truncating the Karhunen–Loève expansion at $n_{KL} = 5$ terms.

The statistical moments of the drag are, therefore, determined for a discretization in an up to ten-dimensional probability space with $n_{KL} = \{1, 2, 3, 5, 10\}$, see Fig. 9e, f. As a result of the slower convergence for the mean drag with an increasing number of KL-expansion terms, the result for $n_{KL} = 10$ is not yet converged for $n_s = 50$. The results for $n_{KL} = 5$ converge to a mean drag of $\mu_D = 0.8555$N, which is only 0.34% larger than the deterministic drag.

The standard deviation of $\sigma_D = 0.05008$N for $n_{KL} = 10$ and $n_s = 50$ is also significantly lower than the values for the fully and strongly correlated cases. The lower variation is caused by the cancelation of the effect of small-scale velocity fluctuations in determining the drag integral quantity. The truncation of the KL expansion also contributes to a lower predicted drag variation.

Another practical difficulty is the accurate convection of the free-stream velocity fluctuations from the inflow boundary to the wing geometry. The usually coarse mesh size in the far field domain would dissipate the imposed spatial variations to a large extent before they reach the wing. Large computational meshes are, therefore, required with a fine mesh discretization upstream of the wing.

5 Conclusions

Recently, the first extremum diminishing uncertainty quantification method for the robust approximation of discontinuous response surfaces without overshoots and undershoots was developed. This multielement approach was, however, limited to finite parameter domains, which can through arbitrary truncation of probability distributions with infinite support result in stochastic bias error. In this paper, the extension of the extremum diminishing concept to infinite parameter ranges in probability space is studied. An approach for infinite parameter domains is developed based on an extremum conserving interpolation of deterministic samples using inverse distance weighting (IDW) interpolation.

This extremum diminishing uncertainty quantification formulation is employed to resolve the effect of 0.5% transonic free-stream velocity fluctuations in the highly sensitive AGARD 445.6 wing test case. For this application, the power parameter limit value $c \to \infty$ is selected in combination with Halton sampling based on results for three analytical test functions with one and two random parameters. A fully correlated velocity field results in the largest effect compared to the deterministic prediction with a 1.75% higher mean wave drag and an amplification of randomness by a factor 19.2 to a wave drag coefficient of variation of $cv_D = 9.58\%$.

The cases with strong and weak spatial correlation of the velocity field modeled by a Karhunen–Loève expansion with up to ten random parameters result in lower mean drag and standard deviation due to the truncation of the Karhunen–Loève expansion and the cancelation of spatial variations in determining an integral quantity such as the drag. Modeling spatial correlation in the free-stream conditions poses specific practical challenges due to the relatively small relevant correlation length compared to the flow domain dimensions and a fine computational mesh for convecting the inflow variations accurately to the wing structure.

The first order error convergence results for extremum diminishing uncertainty quantification on infinite parameter domains for the analytical test problems show that the robustness of the extremum diminishing concept can compromise the efficiency of uncertainty quantification for infinite parameter ranges. More advanced robustness criteria may, therefore, be necessary to obtain a more practical balance between approximation robustness and simulation efficiency. Future work will also include the uncertainty analysis of transonic flows based on viscous flow computations using extensions of IDW interpolation by selecting nearby points and including direction and slope.

References

1. Babuška, I., Tempone, R., Zouraris, G.E.: Galerkin finite element approximations of stochastic elliptic partial differential equations. SIAM J. Numer. Anal. **42**, 800–825 (2004)
2. Babuška, I., Nobile, F., Tempone, R.: A stochastic collocation method for elliptic partial differential equations with random input data. SIAM J. Numer. Anal. **45**, 1005–1034 (2007)
3. Bartier, P.M., Keller, C.P.: Multivariate interpolation to incorporate thematic surface data using inverse distance weighting (IDW). Comput. Geosci. **22**, 795–799 (1996)
4. Bowen, G.J., Revenaugh, J.: Interpolating the isotopic composition of modern meteoric precipitation. Water Resour. Res. **39**, 1299 (2003)
5. Chorin, A.J., Marsden, J.E.: A Mathematical Introduction to Fluid Mechanics. Springer, New York (1979)
6. Cressman, G.P.: An operational objective analysis system. Mon. Weather Rev. **87**, 367–374 (1959)
7. Deb, M., Babuška, I., Oden, J.: Solution of stochastic partial differential equations using Galerkin finite element techniques. Comput. Methods Appl. Mech. Eng. **190**, 6359–6372 (2001)
8. Ghanem, R.G., Spanos, P.: Stochastic Finite Elements: A Spectral Approach. Springer–Verlag, New York (1991)
9. Ghanem, R.: Ingredients for a general purpose stochastic finite elements implementation. Comput. Method. Appl. M. **168**, 19–34 (1999)
10. Hammersley, J.M., Handscomb, D.C.: Monte Carlo Methods. Methuen's monographs on applied probability and statistics. Fletcher & Son Ltd., Norwich (1964)
11. Hosder, S., Walters, R.W. Perez, R.: A non–intrusive polynomial chaos method for uncertainty propagation in CFD simulations. In: Proceedings of the 44th AIAA Aerospace Sciences Meeting and Exhibit, Reno, Nevada, AIAA–2006–891 (2006)
12. Hosder, S., Walters, R.W., Balch, M., Efficient sampling for non–intrusive polynomial chaos applications with multiple uncertain input variables. In: Proceedings of the 48th AIAA/ASME/ASCE/AHS/ASC Structures, Structural Dynamics, and Materials Conference, Honolulu, Hawaii, AIAA–2007–1939 (2007)
13. Jameson, A.: Positive schemes and shock modelling for compressible flows. Int. J. Num. Meth. Fluids **20**, 743–776 (1995)
14. Koobus, B., Farhat, C.: Second-order time-accurate and geometrically conservative implicit schemes for flow computations on unstructured dynamic meshes. Comput. Methods Appl. Mech. Engrg. **170**, 103–129 (1999)
15. Loève, M.: Probability Theory, fourth ed. Springer–Verlag, New York (1977)
16. Loeven, G.J.A., Bijl, H.: Probabilistic collocation used in a two–step approach for efficient uncertainty quantification in computational fluid dynamics. CMES **36**, 193–212 (2008)
17. Le Maître, O.P., Knio, O.M., Najm, H.N., Ghanem, R.G.: A stochastic projection method for fluid flow: I. Basic formulation. J. Comput. Phys. **173**, 481–511 (2001)
18. Le Maître, O.P., Reagan, M.T., Najm, H.N., Ghanem, R.G., Knio, O.M.: A stochastic projection for fluid flow: II. Random process. J. Comput. Phys. **181**, 9–44 (2002)
19. Le Maître, O.P., Najm, H.N., Ghanem, R.G., Knio, O.M.: Multi–resolution analysis of Wiener–type uncertainty propagation schemes. J. Comput. Phys. **197**, 502–531 (2004)
20. Mathelin, L., Hussaini, M.Y., Zang, T.A., Bataille, F.: Uncertainty propagation for a turbulent, compressible nozzle flow using stochastic methods. AIAA J. **42**, 1669–1676 (2004)
21. Mathelin, L., Hussaini, M.Y., Zang, Th.A.: Stochastic approaches to uncertainty quantification in CFD simulations. Num. Alg. **38**, 209–236 (2005)
22. Mathelin, L., Le Maître, O.: Dual–based a posteriori error estimate for stochastic finite element methods. Comm. App. Math. Comput. Sci. **2**, 83–115 (2007)
23. Melchers, R.E.: Structural Reliability: Analysis and Prediction. Wiley, New York (1987)
24. Najm, H.N.: Uncertainty quantification and polynomial chaos techniques in computational fluid dynamics. Annu. Rev. Fluid Mech. **41**, 35–52 (2009)
25. Nellner, P.-Ch., Zierep, J.: A local solution method for shock boundary–layer interaction on a swept wing. Acta Mech. **101**, 45–57 (1993)
26. Okabe, A., Boots, B., Sugihara, K.: Spatial Tessellations: Concepts and Applications of Voronoi Diagrams. Wiley, Chichester, New York (1992)
27. Reagan, M.T., Najm, H.N., Ghanem, R.G., Knio, O.M.: Uncertainty quantification in reacting–flow simulations through non–intrusive spectral projection. Combust. Flame **132**, 545–555 (2003)
28. Shepard, D.: A two–dimensional interpolation function for irregularly–spaced data. In: Proceedings of the 1968 ACM National Conference, 517–524 (1968)
29. Tatang, M.A.: Direct Incorporation of Uncertainty in Chemical and Environmental Engineering Systems. PhD thesis, MIT, Cambridge (1995)
30. Wan, X., Karniadakis, G.E.: An adaptive multi–element generalized polynomial chaos method for stochastic differential equations. J. Comput. Phys. **209**, 617–642 (2005)
31. Wiener, N.: The homogeneous chaos. Am. J. Math. **60**, 897–936 (1938)
32. Witteveen, J.A.S., Bijl, H.: A monomial chaos approach for efficient uncertainty quantification in nonlinear problems. SIAM J. Sci. Comput. **30**, 1296–1317 (2008)
33. Witteveen, J.A.S., Bijl, H.: Effect of randomness on multi-frequency aeroelastic responses resolved by unsteady adaptive stochastic finite elements. J. Comput. Phys. **228**, 7025–7045 (2009)
34. Witteveen, J.A.S., Loeven, G.J.A., Bijl, H.: An adaptive stochastic finite elements approach based on Newton–Cotes quadrature in simplex elements. Comput. Fluids **38**, 1270–1288 (2009)
35. Witteveen, J.A.S., Bijl, H.: A TVD uncertainty quantification method with bounded error applied to transonic airfoil flutter. Commun. Comput. Phys. **6**, 406–432 (2009)
36. Xiu, D., Karniadakis, G.E.: The Wiener–Askey polynomial chaos for stochastic differential equations. SIAM J. Sci. Comput. **24**, 619–644 (2002)

37. Xiu, D., Lucor, D., Su, C.,-H., Karniadakis, G.E.: Stochastic modeling of flow–structure interactions using generalized polynomial chaos. J. Fluid. Eng. **124**, 51–59 (2002)
38. Xiu, D., Karniadakis, G.E.: Modeling uncertainty in flow simulations via generalized polynomial chaos. J. Comput. Phys. **187**, 137–167 (2003)
39. Xiu, D.: Fast numerical methods for stochastic computations: A review. Commun. Comput. Phys. **5**, 242–272 (2009)
40. Yates, E. Jr.: AGARD Standard Aeroelastic Configurations for Dynamic Response. Candidate Configuration I.–Wing 445.6. Technical Memorandum 100492, NASA (1987)
41. Van Zuijlen, A.H., De Boer, A., Bijl, H.: Higher-order time integration through smooth mesh deformation for 3D fluid-structure interaction simulations. J. Comput. Phys. **224**, 414–430 (2007)